Cytoplasmic streaming drifts the polarity cue and enables posteriorization of the *Caenorhabditis elegans* zygote at the side opposite of sperm entry

Kenji Kimura[a,b,*] and Akatsuki Kimura[a,c]
[a]Cell Architecture Laboratory, Structural Biology Center, National Institute of Genetics, Mishima 411-8540, Japan; [b]Department of Biological Science, Kwansei Gakuin University, Sanda 669-1337, Japan; [c]Department of Genetics, School of Life Science, The Graduate University for Advanced Studies, SOKENDAI, Mishima 411-8540, Japan

ABSTRACT **Cell polarization is required to define body axes during development. The position of spatial cues for polarization is critical to direct the body axes. In *Caenorhabditis elegans* zygotes, the sperm-derived pronucleus/centrosome complex (SPCC) serves as the spatial cue to specify the anterior-posterior axis. Approximately 30 min after fertilization, the contractility of the cell cortex is relaxed near the SPCC, which is the earliest sign of polarization and called symmetry breaking (SB). It is unclear how the position of SPCC at SB is determined after fertilization. Here, we show that SPCC drifts dynamically through the cell-wide flow of the cytoplasm, called meiotic cytoplasmic streaming. This flow occasionally brings SPCC to the opposite side of the sperm entry site before SB. Our results demonstrate that cytoplasmic flow determines stochastically the position of the spatial cue of the body axis, even in an organism like *C. elegans* for which development is stereotyped.**

Monitoring Editor
Karen Oegema
University of California, San Diego

Received: Jan 22, 2020
Revised: May 15, 2020
Accepted: May 19, 2020

INTRODUCTION

Cell polarization is a fundamental step in animal development; asymmetric distribution of the determinants of cell fate within a cell establishes the cell polarity. Unidirectionally reinforced transport of polarity determinants through a well-organized cytoskeleton contributes in establishing the polarity in many cases (Munro *et al.*, 2004; Weaver and Kimelman, 2004; Sardet *et al.*, 2007; Prodon *et al.*, 2008; Parton *et al.*, 2011). Internal or external cues that induce cell polarization such as the sperm entry site, the sperm-derived aster, or surrounding cells provide positional information for the proper orientation of embryonic polarity (Ajduk and Zernicka-Goetz, 2016; Chen *et al.*, 2018). The zygotes of *Caenorhabditis elegans* present a paradigm for polarization in which the sperm-derived pronucleus/centrosome complex (SPCC) possesses cues that establish the anterior-posterior (AP) polarity (Goldstein and Hird, 1996).

In *C. elegans* zygotes, the position of SPCC at the time of "symmetry breaking" (SB) is known to determine the AP polarity. SB occurs approximately 30 min after fertilization when local relaxation of contractility of the cell cortex in the vicinity of SPCC occurs, which is the earliest sign of the establishment of the AP polarity (O'Connell *et al.*, 2000; Bienkowska and Cowan, 2012). At this time, Aurora A kinase (AIR-1) relocates from the cytoplasm to the centrosomes (Klinkert *et al.*, 2019; Reich *et al.*, 2019; Zhao *et al.*, 2019). The local relaxation triggers unidirectional advection of the cortical actomyosin that brings the anterior PAR proteins to the future anterior cortex, and simultaneously the posterior PAR proteins are allowed to localize to the future posterior cortex (Munro *et al.*, 2004; Motegi and Sugimoto, 2006). Additionally, within the inner cytoplasm, a flow is generated in a counterdirection to the cortical advection (Niwayama *et al.*, 2011), which potentially promotes loading of the posterior PAR proteins to the future posterior cortex and enforces the formation of the posterior domain (Mittasch *et al.*, 2018). Concomitantly, the actomyosin-dependent flow facilitates the transport of SPCC to

This article was published online ahead of print in MBoC in Press (http://www.molbiolcell.org/cgi/doi/10.1091/mbc.E20-01-0058) on May 27, 2020.
Author contributions: K.K. conceived the study and performed all the experiments; K.K. and A.K. analyzed data and wrote the manuscript.
Competing interests: The authors declare no competing or financial interests.
*Address correspondence to: Kenji Kimura (kekimura@kwansei.ac.jp).
Abbreviations used: AP, anterior-posterior; MeiCS, meiotic cytoplasmic streaming; SB, symmetry breaking; SPCC, sperm-derived pronucleus/centrosome complex.

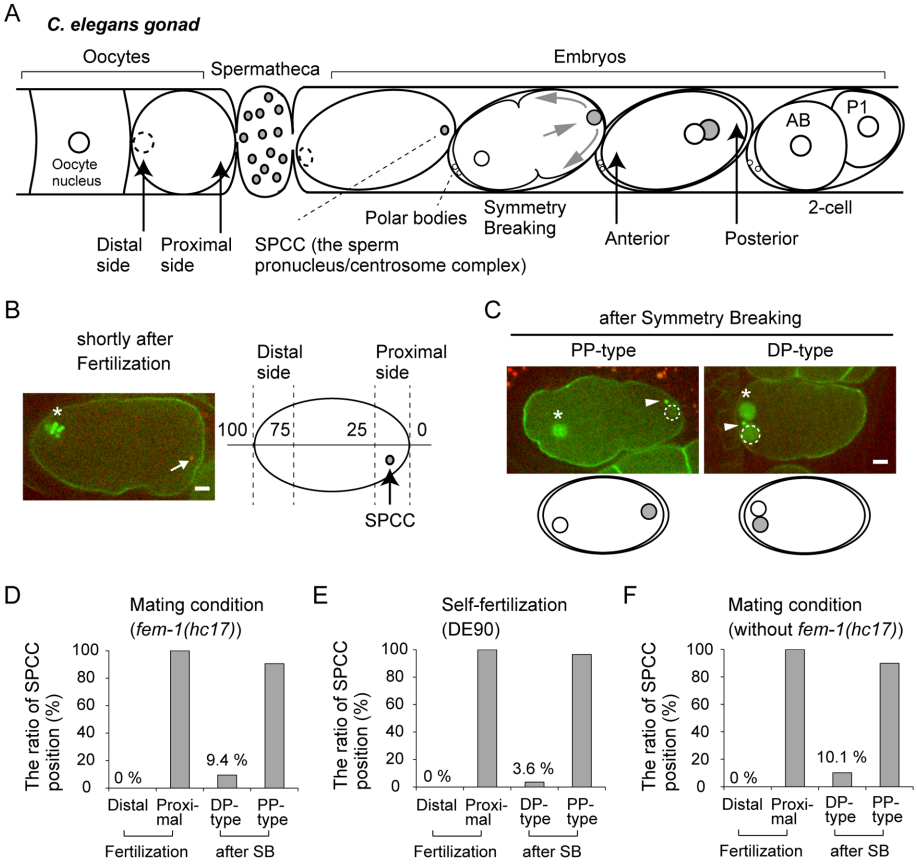

FIGURE 1: The sperm enters only through the proximal side of the oocyte. (A) Schematic of the *C. elegans* gonad and the definition of the proximal and distal sides. (B) Fluorescence confocal image of zygote expressing GFP::PH, GFP::histone and TBG-1::GFP in a *fer-1(hc17)* hermaphrodite crossed to a *him-5(e1490)* male expressing mCherry::histone at a time immediately after fertilization. Asterisks indicate the oocyte-derived chromosomes. The white arrow indicates the position of the SPCC. The distal quartile and proximal quartile of the oocyte or zygote before polarization are defined as the distal and proximal sides, respectively, as shown in the right schematic. Scale bar, 5 µm. (C) Representative examples of the PP and DP-type after SB. Arrowheads indicate the centrosome. White dotted circles indicate the sperm pronucleus. Scale bar, 5 µm. (D–F) The ratios of the zygote of which SPCC is positioned in the distal or proximal side immediately after fertilization and after SB under conditions of (D) mating using CAL0182 (*fer-1(hc17)* mutant) hermaphrodites and CAL0841 males, (E) self-fertilization (DE90), and (F) mating using CAL1041 hermaphrodites and CAL1651 males are shown; $n = 52$ and 53 (D), 89 and 84 (E), and 51 and 69 (F) for each time point, respectively.

the closer pole of the zygote's long axis (Goldstein and Hird, 1996; Bienkowska and Cowan, 2012). As a result, the side containing SPCC becomes the posterior end, while the opposite side becomes the anterior end of the organism. Thus, the position of SPCC at SB defines AP polarity in *C. elegans* zygotes.

How the position of the spatial cue (SPCC) at SB is determined is a critical question to understand the mechanism of polarity specification. The clear answer, however, has not been obtained yet. Since SPCC is derived from the sperm, the site of sperm entry is suspected to have a critical role. In fact, the site of sperm entry seems to correlate with the position of SPCC at SB and thus with the future posterior pole (Goldstein and Hird, 1996). In the *C. elegans* hermaphrodites, the sperm usually fuses with the leading edge of the oocyte, migrating into a sperm storage organ (spermatheca) (Ward and Carrel, 1979; Samuel *et al.*, 2001). We refer to the side of the leading edge as the proximal side, and the opposite side as the distal side (Figure 1A). Since the oocyte nucleus is positioned at the distal side in oocytes, where the polar body extrusions occur after fertilization, the distal side is marked by the position of the first polar body (Figure 1, A and B). In most cases, the proximal side becomes the posterior of the zygote. We call this "PP-type polarization" (Figure 1C). Importantly, the correlation between the proximal side of the oocyte and the posterior of the zygote is not perfect. In some cases, the distal side becomes the posterior (as in "DP-type polarization," Figure 1C). DP-type polarization was observed when a spermless hermaphrodite (*fem-1(hc17)* strain) was mated with wild-type males (Goldstein and Hird, 1996). This treatment was considered to alter the position of sperm entry and increased the chance for the sperm to enter from the distal side of the oocyte. This scenario is based on two assumptions as follows: 1) the sperm can enter from both proximal and distal sides of the oocyte, and 2) SPCC does not move much until SB after fertilization. However, it was unclear whether the sperm actually entered from the distal side when DP-type polarization occurred. The previous observation was based on Nomarski optics, and the position of sperm entry was judged by the position where the sperm pronucleus becomes visible, which is approximately 30 min after fertilization. It is not clear as to how much the SPCC moves in the zygotes during the 30-min period after fertilization. Therefore, it remains unclear how the position of SPCC at SB is determined.

The movements of SPCC after fertilization have been described previously. Before the onset of SB, SPCC is often found at a distant location from the cortex (Bienkowska and Cowan, 2012), indicating that SPCC moves from the sperm entry site, which should be at the cortex. The internally located SPCC then moves toward the cortex on SB (Bienkowska and Cowan, 2012). Furthermore, Panzica *et al.* (2017) observed extensive movement of SPCC when they knocked down profilin (*pfn-1*), which is critical for actin polymerization (Panzica *et al.*, 2017), suggesting that, in normal conditions, the movement of SPCC is suppressed in an actin-dependent manner. Interestingly, a collective flow of the cytoplasm, referred to as meiotic cytoplasmic streaming (MeiCS) (Yang *et al.*, 2003; McNally *et al.*, 2010; Kimura *et al.*, 2017), has been implicated in the movement of SPCC after fertilization. MeiCS is driven by kinesin-1/UNC-116 (McNally *et al.*, 2010). Kinesin-1 is required for the inward positioning of SPCC (McNally *et al.*, 2012) and extensive movement of SPCC in *pfn-1* (RNAi) conditions (Panzica *et al.*, 2017). However, it has not been made clear to what extent MeiCS transports SPCC before SB in normal conditions. More specifically, it is important to determine if MeiCS is capable of moving SPCC to the opposite side of the zygote from the sperm entry site to induce posteriorization (i.e., DP-type polarization).

In this study, we investigated the influence of MeiCS on the dynamics of SPCC before the onset of polarity establishment. Our extensive observations on the position of SPCC after fertilization

reveal that cytoplasmic streaming drastically influences the position of SPCC before SB and has a deterministic role in AP polarity.

RESULTS

The sperm enters only through the proximal side of the oocyte

To clarify the position of sperm entry and of sperm-derived chromosomes after fertilization, we conducted a time-lapse imaging of the zygote produced under the mating condition using the *fem-1(hc17)* strain (Figure 1B), following the procedure described previously (Goldstein and Hird, 1996). We visualized the chromosomes of the *fem-1(hc17)* oocyte by using a green fluorescent protein fused to the histone protein (GFP::histone) under the control of *pie-1* promoter and visualized the sperm-derived chromosomes derived from a male by using a red fluorescent protein (mCherry::histone) under the control of *spe-11* promoter. To obtain males efficiently, we utilized the *him-5(e1490)* mutant that produces male progeny at an increased frequency (Hodgkin *et al.*, 1979). Consistent with the results of the previous study (Goldstein and Hird, 1996), we obtained zygotes with the DP-type polarization at 9.4% frequency (5/53 embryos; Figure 1D). More specifically, the sperm-derived chromosomes were positioned in the distal area (75–100% along the long axis of the zygote; Figure 1B) at a timing known as SB which is the timing of the earliest sign of polarity establishment (i.e., the local relaxation of cortical contractility) and is approximately 30 min after fertilization.

Unexpectedly, under the same mating condition as in the previous study (Goldstein and Hird, 1996), all sperm cells entered from the proximal side (52 embryos); SPCC was found within the range of 0–25% in all cases immediately after fertilization (Figure 1D). This frequency (0/52) was significantly lower ($p = 0.0058$) than the frequency of observing the DP-type polarization (5/53). Moreover, we determined the sperm entry site from the earliest signal of *spe-11p*::mCherry::histone by imaging the oocyte before or immediately after ovulation. The timing and position agreed with those judged from GFP::PH signal (Supplemental Movie S1), which was shown to reflect the fertilization timing and sperm entry site (Takayama and Onami, 2016). Thus, our live-cell imaging indicates that the site of sperm entry is consistently on the proximal side even in the case of DP-type polarization.

To demonstrate that the DP-type polarization is not only observed in the *fem-1* mutant, we also conducted experiments using nonmutant strains ("wild-type," but encodes fluorescently labeled proteins). The DP-type polarization was observed both in the self-fertilization and in the mating conditions (Figure 1, E and F; 3.6% [3/84] and 10.1% [7/69], respectively) with no statistically significant differences observed in the ratio of DP-type polarization occurring between the two conditions ($p > 0.10$). Importantly, also under these conditions, the site of sperm entry was consistently at the proximal side (Figure 1E [89 embryos], Figure 1F [51 embryos]). This result is the first clear demonstration that the sperm does not enter from the distal side of the oocyte and that the site of sperm entry does not specify the posterior pole in the *C. elegans* zygote.

SPCC occasionally moves away from the sperm entry point after fertilization

The earliest sign of polarity establishment is the local relaxation of cortical contractility observed at the time of SB, which is ~30 min after the fertilization. The relaxation occurs at the nearest cortex of the centrosomes associated with SPCC (O'Connell *et al.*, 2000; Bienkowska and Cowan, 2012). Consistent with this view, when the DP-type polarization occurs, SPCC is observed in the distal side on SB (Figure 1C) (Goldstein and Hird, 1996). In contrast, for the DP-type polarization, the sperm entry site does not coincide with the posterior pole and the position of SPCC at SB. This disagreement inevitably suggested that SPCC moved from the sperm entry site (i.e., the proximal side) to the distal side for the DP-type polarization. We succeeded in directly demonstrating that this is actually the case, by optimizing the image acquisition condition to track the position of SPCC at short time intervals, with less photobleaching (Figure 2A; Supplemental Movie S2). We quantified the position along the long axis of the zygote from the images (Figure 2B). When the zygotes conduct the DP-type polarization, SPCC starts from the proximal side and drifts to the distal side after fertilization (Figure 2A, lower; Supplemental Movies S1 and S3; Figure 2C, red symbols and lines). This observation indicates that the position of the spatial cue of polarity (SPCC) is stochastically changed from the sperm entry site before polarity establishment (SB).

Another interesting observation is that, even for the PP-type polarization in which the sperm entry site coincides with the posterior pole, some SPCC moved dynamically to an almost indistinguishable level that causes the DP-type polarization until meiotic anaphase II (Figure 2C, blue symbols and lines). We evaluated the distribution of the position of SPCC at the time of fertilization, meiotic anaphase I, meiotic anaphase II, SB, and immediately before pronuclear migration from all our tracking data. Immediately after fertilization, all SPCCs were found within the proximal side (0–25%) (Figure 2D). A subset of SPCCs was positioned beyond one-quarter of the long axis from the proximal pole (x-position ≥ 25%, Figure 2B) at meiotic anaphase I, which is approximately 10 min after fertilization (Figure 2D). Still others moved further toward the distal side resulting in a wide range of SPCC distribution at SB (Figure 2D). In contrast, majority of SPCCs were positioned within one-quarter of the long axis (x-position < 25%) throughout the period from fertilization to the onset of male pronuclear migration (61% and 68% under the self-fertilization and mating conditions, respectively; two examples are shown in the orange plots in Figure 2C). To determine what causes these motility differences in SPCCs, we plotted the positional distribution of SPCCs that exceeded one-quarter of the long axis at least once before SB (Figure 2E, right panel, >25%). Results show that the ratio of SPCCs traveling beyond one-quarter of the long axis was 42% at meiotic anaphase I and 71% approximately 5 min after meiotic anaphase I (Figure 2E). These results suggest that the dynamics of the SPCC subpopulations were established primarily around meiotic anaphase I. In summary, based on the results of tracking analyses, we provide direct evidence that SPCCs occasionally move from the proximal side to the distal side to induce DP-type polarization. The analyses also suggested that we cannot predict the polarity until at least around anaphase I, as the movements of SPCC for the PP-type and DP-type polarization are indistinguishable before anaphase I. We will discuss the latter point at a later instance.

MeiCS moves SPCC before SB

It is a pertinent question as to what is driving the dynamic movement of SPCC within the zygote after fertilization. In the *C. elegans* zygote, immediately after fertilization and before SB, a global flow of the cytoplasm called as MeiCS is intermittently generated in a kinesin-1 (*unc-116*)-dependent manner (Yang *et al.*, 2003; McNally *et al.*, 2010; Kimura *et al.*, 2017). We previously deciphered the mechanism of the stochastic emergence and reversal of the flow (Kimura *et al.*, 2017). Since the timing of the movement of SPCC is consistent with that of MeiCS (Figure 2, D and E), we hypothesized that the drift of SPCC depends on MeiCS. Here, we provide two lines of evidence supporting this hypothesis. First, we sought to

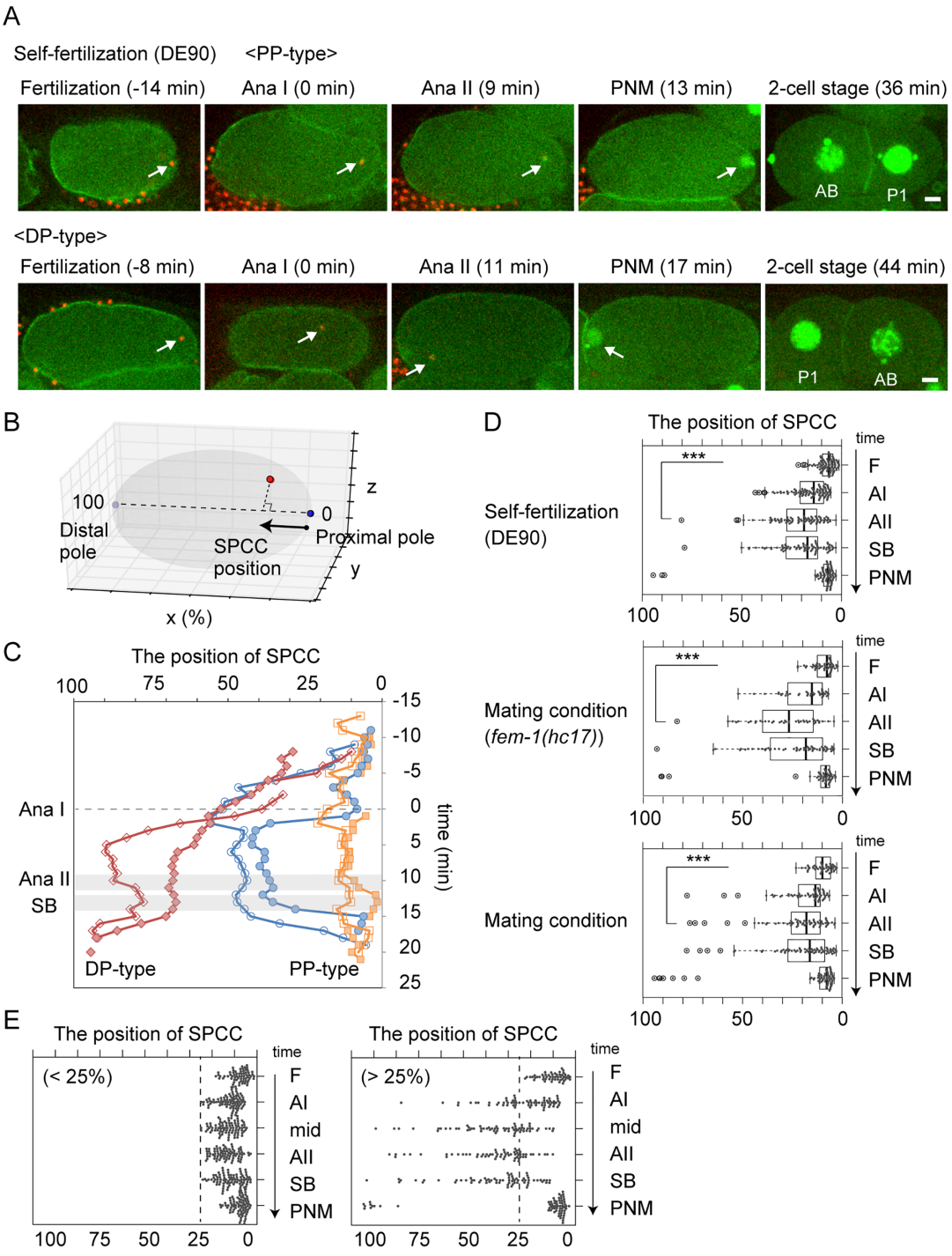

FIGURE 2: SPCC stochastically moves within the zygote before cell polarization. (A) Time series images of *C. elegans* zygotes (DE90 strain) expressing mCherry::histone, GFP::PH, GFP::histone and TBG-1::GFP at fertilization, meiotic anaphase I (Ana I), meiotic anaphase II (Ana II), before pronuclear migration (PNM), and two-cell stage under the condition of self-fertilization. White arrows indicate the position of the SPCC. Representative examples of the DP-type are shown in the bottom panels. The timing of meiotic anaphase I is set to 0 min. Scale bars, 5 μm. (B) The position of SPCC along the long axis of the zygote is evaluated as shown in the diagram and is plotted in C. The proximal pole and the distal pole are set to 0 and 100, respectively. (C) Six representative examples of SPCC dynamics are shown. For details, see the text. (D) Box plots of the position of SPCC along the long axis of the zygote at the timing of fertilization (F), meiotic anaphase I (AI), and meiotic anaphase II (AII), immediately after SB and before pronuclear migration (PNM) under each condition. Asterisks indicate significant differences between F and AII (***$P < 0.001$). (E) Positional distribution of SPCC along the long axis of the zygote which remained within 25% of the long axis (left, <25%) throughout the observation until SB, or exceeded (right, >25%) 25% at least once before SB. SPCCs detected at more than five of the seven time points (F, AI, mid [5 min after AI], AII, SB, PNM) were plotted. Data include both the self-fertilization and mating conditions; $n = 66$, 86, 85, 80, 80, 86, and 83 for each time point in <25%; and $n = 51$, 66, 65, 62, 64, 68, and 66 for each time point in >25%, respectively.

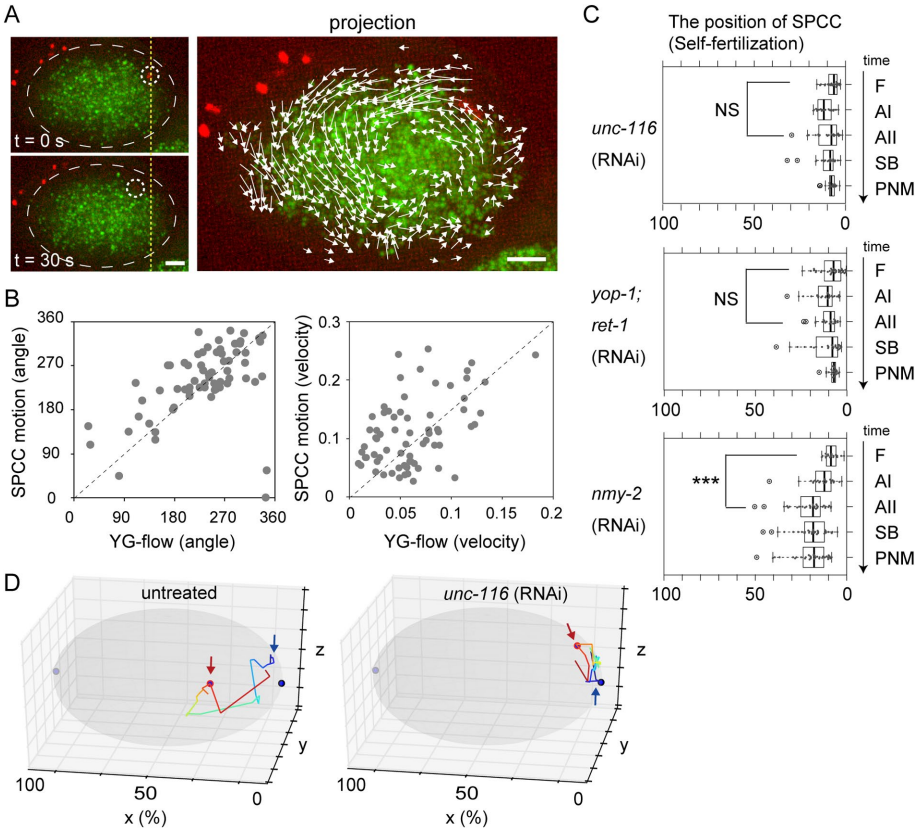

FIGURE 3: MeiCS moves SPCC. (A) The left two panels show time series of *C. elegans* zygote labeled yolk granules (VIT-2::GFP) and SPCC (mCherry::histone). The shape of the zygote is outlined by white dotted line. White dotted circles indicate SPCC. The right panel shows projections of sequential images of the zygote during MeiCS (six frames, time interval: 5 s). White arrows indicate flow vectors of yolk granules (>1 μm). The yellow dotted line indicates the position of SPCC at 0 s. Scale bars, 5 μm. (B) Scatter plots of the angle (degree) and velocity (μm/s) of MeiCS and SPCC motion (69 frames from five zygotes). The mean angle and mean velocity of flow vectors of yolk granules within 7 μm radius of SPCC is calculated as the angle and velocity of MeiCS. (C) Box plots of the position of SPCC along the long axis of the zygote under conditions of *unc-116* RNAi, *yop-1;ret-1* RNAi and *nmy-2* RNAi are shown as in Figure 2D. Asterisks indicate significant differences between F and AII (***$P < 0.001$). NS, not significant. (D) Representative trajectory of SPCC from fertilization to before pronuclear migration in untreated and *unc-116* (RNAi) zygote is shown by the colored line. The gray ellipse represents the zygote and the blue and light blue circle indicates the proximal and distal poles, respectively. The blue arrows indicate the position of fertilization. The red circles with red arrows indicate the position of SPCC at the time of SB.

determine whether the direction of MeiCS is consistent with that of the movement of SPCC. We simultaneously observed SPCC and MeiCS using GFP-labeled yolk granules and found that SPCC moved together with a flow of yolk granules (Figure 3A and Supplemental Movie S4). A correlation was found both in the direction and in the velocity between SPCC movement and the flow of peripheral yolk granules ($r = 0.48$; $P < 0.001$ for both the direction and the velocity, Figure 3B). These results support the idea that MeiCS drives the movement of SPCC before SB. Second, we determined whether the movement of SPCC was suppressed when we attenuated the MeiCS. In *unc-116*/kinesin-1 (RNAi) zygotes, the position of SPCC did not change from the proximal side (Figure 3, C and D). To exclude the possibility that kinesin-1 directly transports SPCC, we also inhibited MeiCS by knockdown of *yop-1;ret-1* genes encoding reticulon proteins are required for the integrity of the ER (Audhya *et al.*, 2007). We previously showed that we can impair the collectivity of MeiCS by fragmenting the ER through *yop-1;ret-1* (RNAi) without inhibiting the motor activity of kinesin-1 (Kimura *et al.*, 2017). As in *unc-116*/kinesin-1 (RNAi) zygotes, the position of SPCC was restricted close to the proximal pole in the *yop-1;ret-1* (RNAi) zygotes (Figure 3C). As a negative control, we impaired the actin-dependent cortical and cytoplasmic flow on SB by knocking down myosin II. In a previous study, it was demonstrated that MeiCS does not require the actin cytoskeleton (McNally *et al.*, 2010). Under this condition, SPCC moved away from the proximal pole before meiotic anaphase II (Figure 3C). These results indicate that MeiCS moves SPCCs from the entry point before SB that sometime causes the DP-type polarization. The DP-type polarization was never observed when MeiCS was impaired ($n = 20$ in *unc-116* [RNAi] zygotes and $n = 23$ in *yop-1;ret-1* [RNAi] zygotes).

The AP axis can be predicted after MeiCS ceases unless SPCC is positioned near the middle of the zygote

At the timing of SB, the earliest sign of polarity (i.e., the local relaxation of cortical contractility) is observed (O'Connell *et al.*, 2000; Bienkowska and Cowan, 2012). The question is how early we can predict the future posterior pole (i.e., distal or proximal of the zygote). The prediction of the posterior may be made earlier than the actual sign of appearance of polarity at SB. We demonstrated that it is not on the sperm entry, but later (Figures 1 and 2). In this study, we demonstrated that MeiCS facilitates the movement of the SPCC (Figure 3), suggesting the possibility that the AP axis is predictable after MeiCS ceases. However, the duration of MeiCS varies from zygote to zygote and is most extensive before meiotic anaphase I, while it generally becomes diminished before meiotic anaphase II (Yang *et al.*, 2003; Panzica *et al.*, 2017).

To more clearly define how early the future posterior pole can be determined, we scored the misprediction rate (Figure 4A), defined as 1) PP-type of which SPCC is positioned within the distal half (x-position: 50–100%) or 2) DP-type of which SPCC is positioned within the proximal half (x-position: 0–50%). The misprediction rate of PP-type was found to be less than 2.5% for all time points. Importantly, the misprediction rate of the DP-type dramatically decreased from 70% at meiotic anaphase I to 18% at 5 min after meiotic anaphase I (mid) and to 9% by meiotic anaphase II. These quantitative results indicate that the posterior position can be predicted once MeiCS ceases.

Next, to specify what kind of cases allow for the prediction of the posterior position at an early point, we constructed histograms of the SPCC position at different stages (Figure 4B). The histogram representing 5 min after anaphase I showed that all SPCCs of DP-type zygotes had already moved to a position more than 45% toward the distal pole. At anaphase II and 1 min before SB, SPCCs located at a

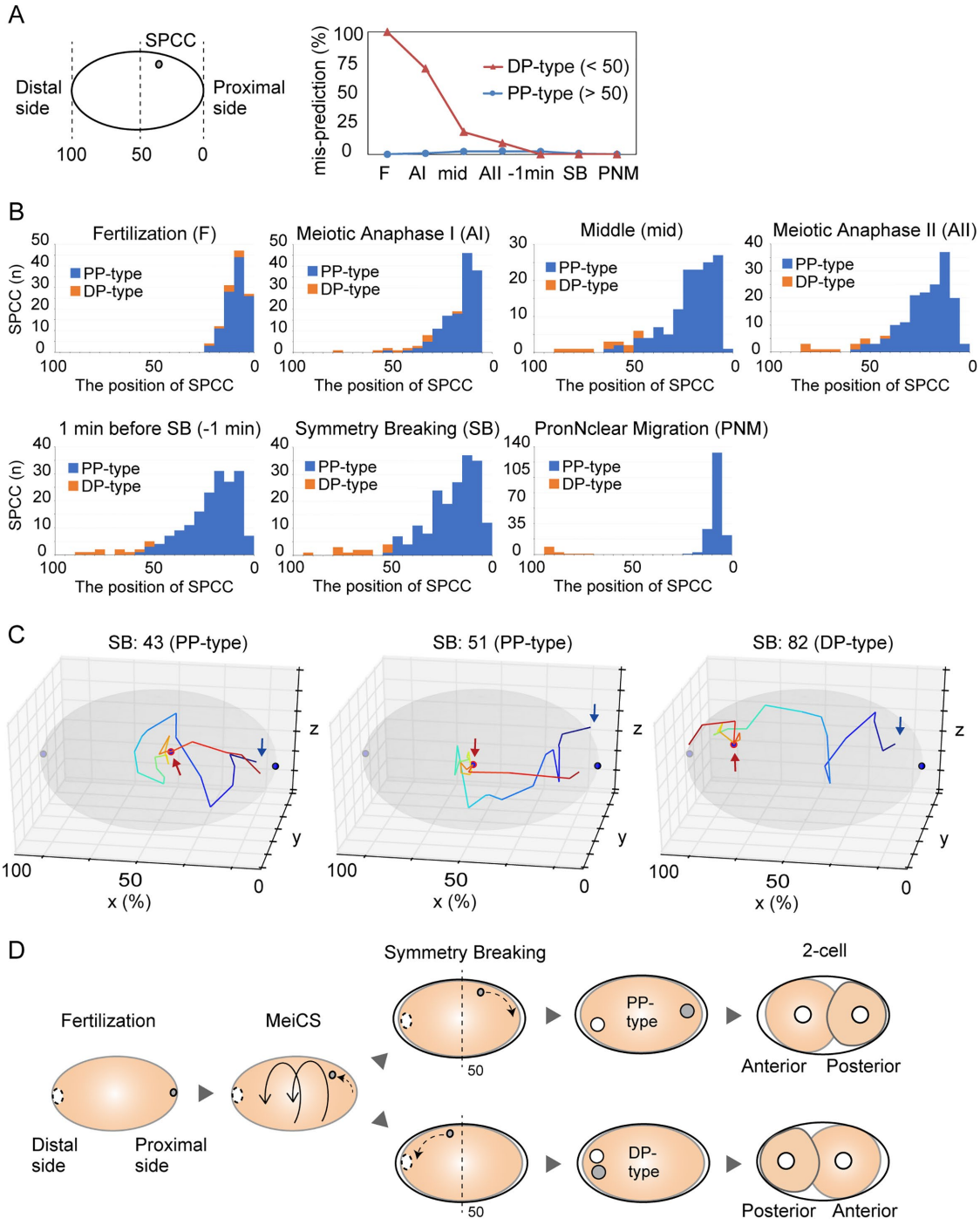

FIGURE 4: The AP axis can be predicted after MeiCS ceases. (A) The frequency of misprediction in PP- and DP-types. For details, refer to the text. (B) Histograms representing the SPCC positions along the long axis of the zygote at the indicated time points for the PP-(blue) and DP-(orange) types; $n = 112$ and 9 (F), 139 and 10 (AI), 134 and 11 (mid), 161 and 11 (AII), 170 and 10 (–1 min), 185 and 12 (SB), and 194 and 16 (PNM) for PP- and DP-types, respectively. (C) Representative trajectories of SPCC in the zygote in which SB occurred when SPCC was positioned at 43, 51, and 82% of the long axis are shown as in Figure 3D. (D) Summary of the SPCC dynamics during cell polarization. For details, see the text.

position >60% toward the distal pole will become DP-type and those located at <40% will become PP-type, whereas for those located between 40 and 60%, the future type cannot be predicted (Figure 4B). However, the future type became predictable at SB for all zygotes except one ($n = 1/199$). Specifically, if the SPCC is located >50% toward the distal pole, the zygote will become DP-type and otherwise PP-type (Figure 4C). The exception was in one PP-type zygote, in which the SPCC was at 51% at SB (Figure 4C). These results indicate that if SPCC is positioned <40% or >60% along the zygotes length 5 min after anaphase I, it can be definitively predicted to be the future posterior aspect. In contrast, if the SPCC is positioned within the 40–60% area, we cannot predict the future posterior aspect until SB.

The inability to predict the future posterior aspect for zygotes with SPCC located in the 40–60% area before SB may be explained by the polarized flow that emerges on SB, which is dependent on actomyosin (Goldstein and Hird, 1996; Munro *et al.*, 2004; Bienkowska and Cowan, 2012). To evaluate the role of the actomyosin flow in this phenomena, we focused on the position of SPCC 1 min before SB, which is before the onset of the polarized flow (Figure 4B). At 1 min before SB, in 2.4% of future PP-type zygotes (n = 4/170), SPCCs remained located in the distal side (51–56% of egg length). Meanwhile, the SPCCs of these four zygotes moved toward the proximal side in the following minute ultimately being located at <50% and the remaining SPCC moved from the 55 to the 51% position. These results suggest that the actomyosin flow facilitated the movement of these SPCCs toward the proximal side. Therefore, if the SPCC is near midcell, the final pole depends on the polarized flow induced at the SB. Since 1) the speed of the flow is less than 0.1 μm/s near the midcell (Niwayama *et al.*, 2011), and 2) for all PP-type zygotes, the SPCC moves to the proximal side at SB (i.e., in less than 1 min), the flow is predicted to play a decisive role for SPCCs positioned less than 6 μm from the center of the zygotes. This estimation is consistent with our observation that SPCC positioned at >50% in the zygotes before the onset of flow moved toward the proximal aspect in up to 7% of the zygote length (~3.5 μm in 1 min) to induce the PP-type polarization.

DISCUSSION

In this study, we revealed how the position of SPCC is determined after fertilization and before the onset of SB in the *C. elegans* zygote. SPCC induces a relaxation of contractility in the nearby cortex causing the SPCC to move toward the closer pole of the now oval-shaped zygote to establish the pole posterior, which is known as posteriorization (Goldstein and Hird, 1996; Bienkowska and Cowan, 2012). Thus, the position of the SPCC at SB determines AP polarity. SPCC is typically positioned in the proximal side of the zygote at SB; however, it is occasionally positioned in the distal side which establishes the distal pole as the posterior end (DP-type). Previously, the DP-type was considered to arise from a sperm entry on the distal side (Goldstein and Hird, 1996). However, we found that the sperm consistently enters from the proximal side of the oocyte; meanwhile, MeiCS drifts SPCC, which occasionally (~10%) results in DP-type polarization. The present study, therefore, indicates that MeiCS has a critical role in the polarization of the AP axis (PP-type or DP-type), and that the position of the spatial cue is determined depending on the stochastic nature of MeiCS before the zygotes proceed to a stereotyped pattern of development (Figure 4D). Is there a benefit for the cell to move SPCC with MeiCS? We believe that the movement of SPCC is a side effect of MeiCS and possibly an unfavorable one. Our previous study suggested that a primary role of MeiCS is to increase the mobility of cortical granules for their efficient exocytosis at the meiotic anaphase I (Kimura *et al.*, 2017). In contrast, the movement of SPCC is considered unfavorable for the cell as it may induce a contact between the oocyte chromosome and the sperm chromosome before the oocyte meiosis (Panzica *et al.*, 2017). The nature of MeiCS is likely designed to move cortical granules efficiently while keeping the movement of SPCC minimum. The flow direction of MeiCS is biased along the short axes of the zygote and, thus, it does not effectively move SPCC along the long axis (Kimura *et al.*, 2017). In addition, MeiCS is not stable and stochastically changes the direction (Kimura *et al.*, 2017), which also makes a long-distance movement difficult. In fact, in the majority of zygotes (~70%), SPCC stayed within the 0–25% proximal side until SB.

Another mechanism to suppress the movement of SPCC by MeiCS is the anchoring of SPCC to the cell cortex (Panzica *et al.*, 2017). Panzica *et al.* (2017) reported that, without the anchoring mechanism, SPCC detaches from the cortex and moves dynamically inside the cell (Panzica *et al.*, 2017). Therefore, the movement of SPCC is likely a result of competition between the stirring effect of MeiCS and the anchoring mechanism. Our present results indicate that the MeiCS overcomes the anchoring mechanism to a certain extent. Even in those cases where the sperm chromosome gets closer to the oocyte chromosomes during the meiosis, we did not observe abnormal meiosis. It has been reported that, in the DP-type polarization, where sperm chromosome should be near to the oocyte chromosomes before meiosis, the embryogenesis is normal (Goldstein and Hird, 1996). Importantly, McNally *et al.* (2012) reported that the depletion of kinesin-1 subunit (KCA-1) promotes premature growth of sperm aster that can occasionally capture the oocyte chromosomes and causes a failure of meiosis (McNally *et al.*, 2012). These results collectively indicate a dual role of the kinesin-1 motor. Kinesin-1 generates MeiCS for efficient cortical granule exocytosis that stochastically leads the DP-polarization. At the same time, kinesin-1 protects sperm chromosomes from mixing with oocyte chromosomes even when they are positioned in the vicinity. These mechanisms should make the mixture of cytoplasm and the integrity of chromosomes compatible. Considering the potential risk of MeiCS moving SPCC, there may be an undiscovered, greater benefit for the cell to conduct MeiCS.

Sperm-derived material provides a polarity cue to a fertilized zygote in some other species besides *C. elegans*. In the ascidian and frog egg, sperm entry or sperm-derived material affects the direction of cortical rotation, which polarizes dorsal determinants toward the opposite side from sperm to specify the dorsal-ventral axis (Roegiers *et al.*, 1995; Weaver and Kimelman, 2004; Houston, 2012). Massive cytoplasmic streaming often occurs after fertilization in many species. In mouse, the site of sperm entry forms an actomyosin-rich cortex called the fertilization cone that generates cytoplasmic flow through rhythmic contractions (Ajduk *et al.*, 2011). The movement of the sperm-derived materials after the fertilization driven by cytoplasmic streaming might be a general phenomenon that may affect the polarization of the zygotes.

MATERIALS AND METHODS

Strains and manipulation of *C. elegans*

C. elegans strains were maintained using the standard techniques (Brenner, 1974). RNAi was performed by injecting double-stranded RNAs, as described previously (Kimura and Kimura, 2012). For the mating experiments, CAL0182 (carrying *fem-1(hc17)*) hermaphrodites (Kondo and Kimura, 2019) were grown at restrictive temperature (25°C) and were mated to CAL0841 (carrying *him-5(e1490)*) males. CAL1041 hermaphrodites were mated to CAL1651 (carrying *him-5(e1490)*) males at 22°C. For the analysis of the SPCC dynamics under self-fertilization condition, DE90 strain was used (Johnston *et al.*, 2010). For the analysis of cytoplasmic streaming, DH1033 strain was used (Grant and Hirsh, 1999). The strains used in this study are listed in Table 1.

Microscopy

Microscopic analysis was performed as described previously (Kimura and Kimura, 2012). Briefly, worms were anesthetized with 1 mM levamisole and mounted on an agar pad. For the tracking analysis of the sperm complex within the zygote, eight or nine different focal planes (Z-interval = 3 μm) were acquired every 30 or 60 s. For the

Name	Genotype	Reference
CAL0182	*fem-1(hc17) IV; unc-119(ed3) III, ruIs32 [pie-1p::GFP::H2B; unc-119(+)] III. ddIs6 [tbg-1::GFP; unc-119(+)] V.*	Kondo and Kimura (2019)
DE90	*oxIs318 [spe-11p::mCherry::histone; unc-119(+)] II; unc-119(ed3 or e2498) ruIs32 III; ddIs6 V; dnIs17.*	Johnston *et al.* (2010)
DH1033	*sqt-1(sc103) II; bIs1 X; bIs1[vit-2::GFP + rol-6(su1006)]*	Grant and Hirsh (1999)
CAL1041	*unc-119(ed3) III; oxIs279 [pie-1p::GFP::H2B; unc-119(+)]., ltIs38[pAA1; pie-1::GFP::PH(PLC1delta1); unc-119(+)]*	This study
CAL0841	*him-5(e1490) V; unc-119(ed3) III; oxIs318 II; unc-119(ed3 or e2498) ruIs32 III; ddIs6 V; dnIs17.*	This study
CAL1651	*him-5(e1490) V; unc-119(ed3) III; oxIs318 II.*	This study

TABLE 1: *C. elegans* strains used in this study.

analysis of the flow field of MeiCS, three different focal planes (Z-interval = 3 μm) were acquired every 5 s.

Image analysis

For tracking analysis of SPCC, the movements of *spe-11p*::mCherry::histone signal, the sperm chromosomal marker, were manually tracked from time-lapse confocal images of the zygotes using Fiji software. To analyze the sperm entry site, we began imaging before or immediately after ovulation (i.e., the oocyte enters the spermatheca) and defined the timing of fertilization as the first time point in which we detected the sperm-derived chromosome in the zygote located in the spermatheca. Furthermore, we defined the sperm entry site as the position of SPCC at fertilization. The timing of fertilization and the position of the sperm entry site with our definition were consistent with those detected from the GFP::PH signal (Takayama and Onami, 2016) (Supplemental Movie S1). We also defined the time of the onset of meiotic chromosomal separation as meiotic anaphase I and II, the time at which the SPCC begins to move linearly to the cortex as the onset of SB, and the time just prior to sperm pronuclear migration as PNM (Figure 2D). For drawing the trajectories of SPCC, we used Matplotlib (Line3DCollection) in a Python library.

For detection of the movements of yolk granules during MeiCS, optical flow analysis was conducted on time-lapse confocal fluorescence images of *C. elegans* zygotes. We used the Farnebäck method implemented in the OpenCV library. All images were rotated so that the long axis of the zygote was parallel to the horizontal axis before the optical flow analysis. To determine the correlation between the SPCC movement and MeiCS (Figure 3B), the mean angle and the mean velocity of the flow of yolk granules within 7 μm from SPCC were analyzed for the period SPCC continuously moved on a single focal plane.

Statistical analysis

The probability that sperm enters the distal side was analyzed using the BINOMDIST function (Microsoft Excel). The two-population z-test was used to analyze the statistical difference between the frequency of the DP-type under self-fertilization and under mating conditions (Figure 1, D–F). The Student's *t* test was used to analyze the statistical difference between the SPCC distribution at fertilization and at meiotic anaphase II (Figures 2D and 3C). A Pearson correlation analysis was used to analyze the correlation between the SPCC movement and the flow of peripheral yolk granules (Figure 3B).

ACKNOWLEDGMENTS

Some strains were provided by the Caenorhabditis Genetics Center, which is funded by National Institutes of Health Office of Research Infrastructure Programs (P40 OD010440). We thank H. Sawa (National Institute of Genetics, Mishima, Japan), F. Motegi (National University of Singapore), and the members of Cell Architecture Laboratory (National Institute of Genetics, Mishima, Japan) for their valuable comments and support. This project was supported by JSPS KAKENHI (grant numbers JP26840072 and JP19K06681 to K.K. and JP16H05119, JP16H00816, JP18H05529, and JP18H02414 to A.K.) and NIG-JOINT (76A2019).

REFERENCES

Ajduk A, Ilozue T, Windsor S, Yu Y, Seres KB, Bomphrey RJ, Tom BD, Swann K, Thomas A, Graham C, *et al.* (2011). Rhythmic actomyosin-driven contractions induced by sperm entry predict mammalian embryo viability. Nat Commun 2, 417.

Ajduk A, Zernicka-Goetz M (2016). Polarity and cell division orientation in the cleavage embryo: from worm to human. Mol Hum Reprod 22, 691–703.

Audhya A, Desai A, Oegema K (2007). A role for Rab5 in structuring the endoplasmic reticulum. J Cell Biol 178, 43–56.

Bienkowska D, Cowan CR (2012). Centrosomes can initiate a polarity axis from any position within one-cell *C. elegans* embryos. Curr Biol 22, 583–589.

Brenner S (1974). The genetics of *Caenorhabditis elegans*. Genetics 77, 71–94.

Chen Q, Shi J, Tao Y, Zernicka-Goetz M (2018). Tracing the origin of heterogeneity and symmetry breaking in the early mammalian embryo. Nat Commun 9, 1819.

Goldstein B, Hird SN (1996). Specification of the anteroposterior axis in *Caenorhabditis elegans*. Development 122, 1467–1474.

Grant B, Hirsh D (1999). Receptor-mediated endocytosis in the *Caenorhabditis elegans* oocyte. Mol Biol Cell 10, 4311–4326.

Hodgkin J, Horvitz HR, Brenner S (1979). Nondisjunction mutants of the nematode *Caenorhabditis elegans*. Genetics 91, 67–94.

Houston DW (2012). Cortical rotation and messenger RNA localization in *Xenopus* axis formation. Wiley Interdiscip Rev Dev Biol 1, 371–388.

Johnston WL, Krizus A, Dennis JW (2010). Eggshell chitin and chitin-interacting proteins prevent polyspermy in *C. elegans*. Curr Biol 20, 1932–1937.

Kimura K, Kimura A (2012). Rab6 is required for the exocytosis of cortical granules and the recruitment of separase to the granules during the oocyte-to-embryo transition in *Caenorhabditis elegans*. J Cell Sci 125, 5897–5905.

Kimura K, Mamane A, Sasaki T, Sato K, Takagi J, Niwayama R, Hufnagel L, Shimamoto Y, Joanny J-F, Uchida S, *et al.* (2017). Endoplasmic-reticulum-mediated microtubule alignment governs cytoplasmic streaming. Nat Cell Biol 19, 399–406.

Klinkert K, Levernier N, Gross P, Gentili C, von Tobel L, Pierron M, Busso C, Herrman S, Grill SW, Kruse K, *et al.* (2019). Aurora A depletion reveals centrosome-independent polarization mechanism in *Caenorhabditis elegans*. Elife 8.

Kondo T, Kimura A (2019). Choice between 1- and 2-furrow cytokinesis in *Caenorhabditis elegans* embryos with tripolar spindles. Mol Biol Cell 30, 2065–2075.

McNally KL, Fabritius AS, Ellefson ML, Flynn JR, Milan JA, McNally FJ (2012). Kinesin-1 prevents capture of the oocyte meiotic spindle by the sperm aster. Dev Cell 22, 788–798.
McNally KL, Martin JL, Ellefson M, McNally FJ (2010). Kinesin-dependent transport results in polarized migration of the nucleus in oocytes and inward movement of yolk granules in meiotic embryos. Dev Biol 339, 126–140.
Mittasch M, Gross P, Nestler M, Fritsch AW, Iserman C, Kar M, Munder M, Voigt A, Alberti S, Grill SW, *et al*. (2018). Non-invasive perturbations of intracellular flow reveal physical principles of cell organization. Nat Cell Biol 20, 344–351.
Motegi F, Sugimoto A (2006). Sequential functioning of the ECT-2 RhoGEF, RHO-1 and CDC-42 establishes cell polarity in Caenorhabditis elegans embryos. Nat Cell Biol 8, 978–985.
Munro E, Nance J, Priess JR (2004). Cortical flows powered by asymmetrical contraction transport PAR proteins to establish and maintain anterior-posterior polarity in the early *C. elegans* embryo. Dev Cell 7, 413–424.
Niwayama R, Shinohara K, Kimura A (2011). Hydrodynamic property of the cytoplasm is sufficient to mediate cytoplasmic streaming in the *Caenorhabditis elegans* embryo. Proc Natl Acad Sci USA 108, 11900–11905.
O'Connell KF, Maxwell KN, White JG (2000). The *spd-2* gene is required for polarization of the anteroposterior axis and formation of the sperm asters in the *Caenorhabditis elegans* zygote. Dev Biol 222, 55–70.
Panzica MT, Marin HC, Reymann AC, McNally FJ (2017). F-actin prevents interaction between sperm DNA and the oocyte meiotic spindle in *C. elegans*. J Cell Biol 216, 2273–2282.
Parton RM, Hamilton RS, Ball G, Yang L, Cullen CF, Lu W, Ohkura H, Davis I (2011). A PAR-1-dependent orientation gradient of dynamic microtubules directs posterior cargo transport in the *Drosophila* oocyte. J Cell Biol 194, 121–135.
Prodon F, Sardet C, Nishida H (2008). Cortical and cytoplasmic flows driven by actin microfilaments polarize the cortical ER-mRNA domain along the a-v axis in ascidian oocytes. Dev Biol 313, 682–699.
Reich JD, Hubatsch L, Illukkumbura R, Peglion F, Bland T, Hirani N, Goehring NW (2019). Regulated activation of the PAR polarity network ensures a timely and specific response to spatial cues. Curr Biol 29, 1911–1923.e1915.
Roegiers F, McDougall A, Sardet C (1995). The sperm entry point defines the orientation of the calcium-induced contraction wave that directs the first phase of cytoplasmic reorganization in the ascidian egg. Development 121, 3457–3466.
Samuel AD, Murthy VN, Hengartner MO (2001). Calcium dynamics during fertilization in *C. elegans*. BMC Dev Biol 1, 8.
Sardet C, Paix A, Prodon F, Dru P, Chenevert J (2007). From oocyte to 16-cell stage: cytoplasmic and cortical reorganizations that pattern the ascidian embryo. Dev Dyn 236, 1716–1731.
Takayama J, Onami S (2016). The sperm TRP-3 channel mediates the onset of a Ca(2+) wave in the fertilized *C. elegans* oocyte. Cell Rep 15, 625–637.
Ward S, Carrel JS (1979). Fertilization and sperm competition in the nematode *Caenorhabditis elegans*. Dev Biol 73, 304–321.
Weaver C, Kimelman D (2004). Move it or lose it: axis specification in *Xenopus*. Development 131, 3491–3499.
Yang HY, McNally K, McNally FJ (2003). MEI-1/katanin is required for translocation of the meiosis I spindle to the oocyte cortex in *C. elegans*. Dev Biol 260, 245–259.
Zhao P, Teng X, Tantirimudalige SN, Nishikawa M, Wohland T, Toyama Y, Motegi F (2019). Aurora-A breaks symmetry in contractile actomyosin networks independently of its role in centrosome maturation. Dev Cell 48, 631–645.